The Plant Cell, Vol. 21: 2118–2132, July 2009, www.plantcell.org

Sieve Element Ca^{2+} Channels as Relay Stations between Remote Stimuli and Sieve Tube Occlusion in *Vicia faba* [W]

Alexandra C.U. Furch,[a] Aart J.E. van Bel,[a] Mark D. Fricker,[b] Hubert H. Felle,[c] Maike Fuchs,[a] and Jens B. Hafke[a,1]

[a] Plant Cell Biology Research Group, Institute of General Botany, Justus-Liebig-University, D-35390 Giessen, Germany
[b] Department of Plant Sciences, University of Oxford, Oxford, OX1 3RB, United Kingdom
[c] Institute of General Botany, Justus-Liebig-University, D-35390 Giessen, Germany

Damage induces remote occlusion of sieve tubes in *Vicia faba* by forisome dispersion, triggered during the passage of an electropotential wave (EPW). This study addresses the role of Ca^{2+} channels and cytosolic Ca^{2+} elevation as a link between EPWs and forisome dispersion. Ca^{2+} channel antagonists affect the initial phase of the EPW as well as the prolonged plateau phase. Resting levels of sieve tube Ca^{2+} of ~50 nM were independently estimated using Ca^{2+}-selective electrodes and a Ca^{2+}-sensitive dye. Transient changes in cytosolic Ca^{2+} were observed in phloem tissue in response to remote stimuli and showed profiles similar to those of EPWs. The measured elevation of Ca^{2+} in sieve tubes was below the threshold necessary for forisome dispersion. Therefore, forisomes need to be associated with Ca^{2+} release sites. We found an association between forisomes and endoplasmic reticulum (ER) at sieve plates and pore-plasmodesma units where high-affinity binding of a fluorescent Ca^{2+} channel blocker mapped an increased density of Ca^{2+} channels. In conclusion, propagation of EPWs in response to remote stimuli is linked to forisome dispersion through transiently high levels of parietal Ca^{2+}, release of which depends on both plasma membrane and ER Ca^{2+} channels.

INTRODUCTION

It has been shown that burning the tip of a *Vicia faba* leaf induces an electropotential wave (EPW) along the sieve tubes that triggers remote sieve tube occlusion by forisome dispersion and subsequent callose production (Furch et al., 2007). Both occlusion processes are known to require free Ca^{2+} for response in vitro (Colombani et al., 2004; Knoblauch et al., 2005). Hence, it was postulated that both occlusion mechanisms may be triggered by influx of Ca^{2+} ions during EPWs.

Long-distance communication by EPWs, initiated by sudden environmental changes, is well established in plants (Stankovic et al., 1998; Stahlberg et al., 2006; Grams et al., 2009). EPWs have been recorded in response to stimuli, such as wounding, cold, heat, and electrical shocks. For example, EPWs were detected after a distant heat stimulus (burning) in *Vitis vinifera* plants (Mancuso, 1999), *Lupinus angustifolius* shoots (Zawadzki and Trebacz, 1982), *Solanum lycopersicum* leaves (Rhodes et al., 1996), and leaf veins of *V. faba* (Furch et al., 2007). Fromm and Spanswick (1993) also recorded EPWs in response to electrical stimulation using microelectrodes impaled blindly into the stem phloem of *Salix viminalis*. These EPWs are thought to propagate mainly along the phloem, in particular along the sieve tubes (Samejima and Sibaoka, 1983; Fromm, 1991; Fromm and Spanswick, 1993; Fromm and Bauer, 1994; Rhodes et al., 1996).

[1] Address correspondence to jens.hafke@bot1.bio.uni-giessen.de.
The author responsible for distribution of materials integral to the findings presented in this article in accordance with the policy described in the Instructions for Authors (www.plantcell.org) is: Jens B. Hafke (jens.hafke@bot1.bio.uni-giessen.de).
[W] Online version contains Web-only data.
www.plantcell.org/cgi/doi/10.1105/tpc.108.063107

The identity of ion channels involved in EPWs is not well characterized, not least because they embody features of both rapid transient action potentials (APs) and slow wave potentials or variation potentials (VPs). In plant APs, the initial depolarization is thought to involve activation of plasma membrane (PM) Ca^{2+} channels (cf. White, 2000; Demidchik and Maathuis, 2007), leading to Ca^{2+} influx, and Ca^{2+}-dependent anion channels (Lunevsky et al., 1983; Felle and Zimmermann, 2007), leading to anion efflux. The recovery phase involves inwardly rectifying K^+ channels (Lunevsky et al., 1983; Fromm and Lautner, 2007). In slow wave potentials or VPs, there may be activation of mechanosensitive Ca^{2+} channels in response to hydraulic pressure waves (Stahlberg and Cosgrove, 1997) and additional shutdown of the PM H^+-pump (Stahlberg et al., 2006), leading to prolonged depolarization (Fromm and Lautner, 2007).

The cell walls of sieve elements (SEs) may act as substantial extracellular Ca^{2+} reservoirs as the apoplast typically contains free Ca^{2+} concentrations in the order of 10^{-4} to 10^{-5} M (Kauss, 1987; Gilroy et al., 1993). Recruitment of Ca^{2+} from the apoplast implies the need for Ca^{2+} channels and Ca^{2+} pumps on the SE plasma membrane (SE-PM). There is some evidence from immunolabeling and fluorescent drug binding studies for nifedipine binding Ca^{2+} channels on the SE-PM of *Nicotiana tabacum* and *Pistia stratiotes* (Volk and Franceschi, 2000).

PM-mediated Ca^{2+} influx can be augmented by release of Ca^{2+} from internal Ca^{2+} stores, such as the endoplasmic reticulum (ER) and vacuole (Sanders et al., 2002). The Ca^{2+} concentration in vacuoles appears to be in the low millimolar range (Felle, 1988), with similar values reported for the ER lumen under resting conditions (Montero et al., 1995). Since SEs are devoid of vacuoles (e.g., van Bel, 2003), the ER is likely to be the main intracellular Ca^{2+} store in SEs (e.g., Sjolund and Shih, 1983).

Indeed, there is a well-developed stacked sieve element reticulum (SER) that appears to be anchored to the SE-PM in clusters in *V. faba* (Ehlers et al., 2000) that could provide a substantial, localized Ca^{2+} reserve. Ca^{2+} release from and reuptake by ER requires the presence of Ca^{2+} channels and Ca^{2+} pumps on the ER membrane (Hong et al., 1999; Sanders et al., 2002).

Local influx of Ca^{2+} along the EPW pathway may trigger intracellular cascades. Sieve tube occlusion would be an example of such a local response provided that the Ca^{2+} gradient is steep enough and Ca^{2+} channel activity allows sufficient Ca^{2+} influx to trigger forisome dispersion and/or callose formation. However, widely divergent free Ca^{2+} concentrations have been reported for sieve tube sap, ranging from micromolar to millimolar (Fromm and Spanswick, 1993; Fromm and Bauer, 1994; Brauer et al., 1998; Knoblauch et al., 2005). In other plant cells, cytosolic free Ca^{2+} concentrations range from 10 to 200 nM and Ca^{2+} elevations during signaling tend to reach the high nanomolar range (Plieth et al., 1999; Trewavas, 1999; Plieth, 2001; Mithöfer and Mazars, 2002; Logan and Knight, 2003). Thus, reports on high free Ca^{2+} concentrations in the SE lumen are difficult to reconcile with established Ca^{2+} signaling paradigms.

Given the presumptive importance of Ca^{2+} homeostasis and signaling for sieve tube physiology, a detailed study on the resting level of Ca^{2+} in SE and Ca^{2+} dynamics during passage of EPWs is required, along with characterization of the possible Ca^{2+} stores and Ca^{2+} channels involved. Thus, we first tested the impact of various Ca^{2+} channel blockers on EPWs induced by distant stimuli and the associate forisome responses. Second, we measured the resting level of free Ca^{2+} in sieve tube sap using both Ca^{2+}-selective electrodes and fluorescent Ca^{2+}-sensitive dyes. Third, we followed changes in free Ca^{2+} concentration during EPWs in intact plants using fluorescent Ca^{2+} dyes and confocal laser scanning microscopy (CLSM). Finally, we characterized the intracellular distribution of Ca^{2+} channels over the SE using fluorescently tagged Ca^{2+} channel blockers and CLSM and the association of forisomes with SER clusters by transmission electron microscopy (TEM).

RESULTS

EPWs and Forisome Dispersion Are Sensitive to Ca^{2+} Channel Blockers

EPWs were recorded using microelectrodes impaled into sieve tubes simultaneously with observation of forisome responses. A wound stimulus, initiated by burning the leaf tip, triggered propagation of EPWs. Seconds after the remote stimulus, the SE-PM transiently depolarized from −140 to −50 mV (Figure 1A). The SE-PM partially repolarized after 60 s to a long-lasting plateau around −90 mV that then gradually returned to resting levels. The magnitude and duration of the plateau phase varied in each measurement before the resting potential was reestablished (n = 10). Prior to the stimulus, the spindle-shaped forisome was typically observed to be closely associated with the sieve plate [Figures 1B(i) to 1B(ii)]. As the peak of the EPW passed, the forisome dispersed shortly (5 to 10 s) after the initial membrane depolarization [Figure 1B(iii)]. To visualize the forisome dynamics more clearly, forisomes were labeled with 5-chloromethyleosin-diacetate (CMEDA)/5-chloromethylfluorescein-diacetate (CMFDA) and observed with CLSM (Figure 1C). Again, a burning stimulus rapidly induced forisome dispersion (n = 12) within ~1 min [Figure 1C(ii)]. Forisomes subsequently recondensed after ~8 to 10 min [Figure 1C(iii)], at the time when the membrane potential was approaching the resting state (Figure 1A). Depolarization of the PM alone in the absence of a wound stimulus by adding 100 mM KCl to a second phloem window 3 to 4 cm upstream from the observation window was not sufficient to trigger a substantial EPW (Figure 1D). Only small depolarizations with amplitudes in the range of 2 to 18 mV were observed, and repolarization took place within 60 s (n = 4). No forisome dispersion was observed under these conditions in bright-field images (Figure 1E) or following fluorescent labeling (Figure 1F, n = 8). Likewise, a more gentle burning stimulus in which the leaf tip was not in contact with the flame only gave a brief depolarization with no plateau phase (n = 5). In this case, the forisome dispersed at both ends, while the mid-section stayed condensed.

To determine whether apoplastic Ca^{2+} influx was required for propagation of EPWs and for forisome dispersion, phloem tissue was preincubated with 2 mM La^{3+}, which is thought to act as a cell-impermeant Ca^{2+} channel blocker as described for animal systems (Hille, 1992). The electrical signal showed a pronounced reduction in amplitude of the initial depolarization by 50 to 70% for La^{3+} (Figure 1G, n = 3). La^{3+}, as well as Gd^{3+} (see Supplemental Figure 1 online), was also sufficient to inhibit forisome dispersion in response to remote burning stimuli (Figure 1H, n = 10) or osmotic shocks (500 mM mannitol, n = 3) in intact phloem tissue.

The effect of the animal L-type Ca^{2+} channel blockers nifedipine and verapamil were also investigated. Nifedipine at 250 μM was sufficient to inhibit depolarization in response to burning by 30 to 50% at the peak and reduce the plateau phase (Figure 1I, n = 3). Furthermore, nifedipine inhibits the forisome dispersion (Figure 1J). Responses to verapamil (n = 4) were more complex. Verapamil hyperpolarized the resting membrane potential in a concentration-dependent manner (Figure 1K) and inhibited forisome dispersion (see Supplemental Figure 2 online). The initial transient depolarization in response to burning was reduced. However, the plateau phase was prolonged and in some cases showed a subsequent increase accompanied by breakdown of the membrane potential (Figure 1L, 500 μM verapamil, black trace).

Confocal Imaging of Ca^{2+} Dynamics in Intact SEs

The effect of different Ca^{2+} channel inhibitors was consistent with a role for Ca^{2+} influx in response to remote stimuli for both EPW propagation and forisome dispersion. To test whether Ca^{2+} increases in the sieve element/companion cell (SE/CC) complex could be observed directly, we measured changes in fluorescence from the single-wavelength fluorescent Ca^{2+} indicators Oregon Green 488-BAPTA-1 (OGB-1) or Fluo-3, loaded as either acetoxymethyl (AM) esters in the presence of Pluronic F127 or at low pH (pH 4.3) in their free acid form (Fricker et al., 1999; Camacho et al., 2000). Both methods were effective in loading

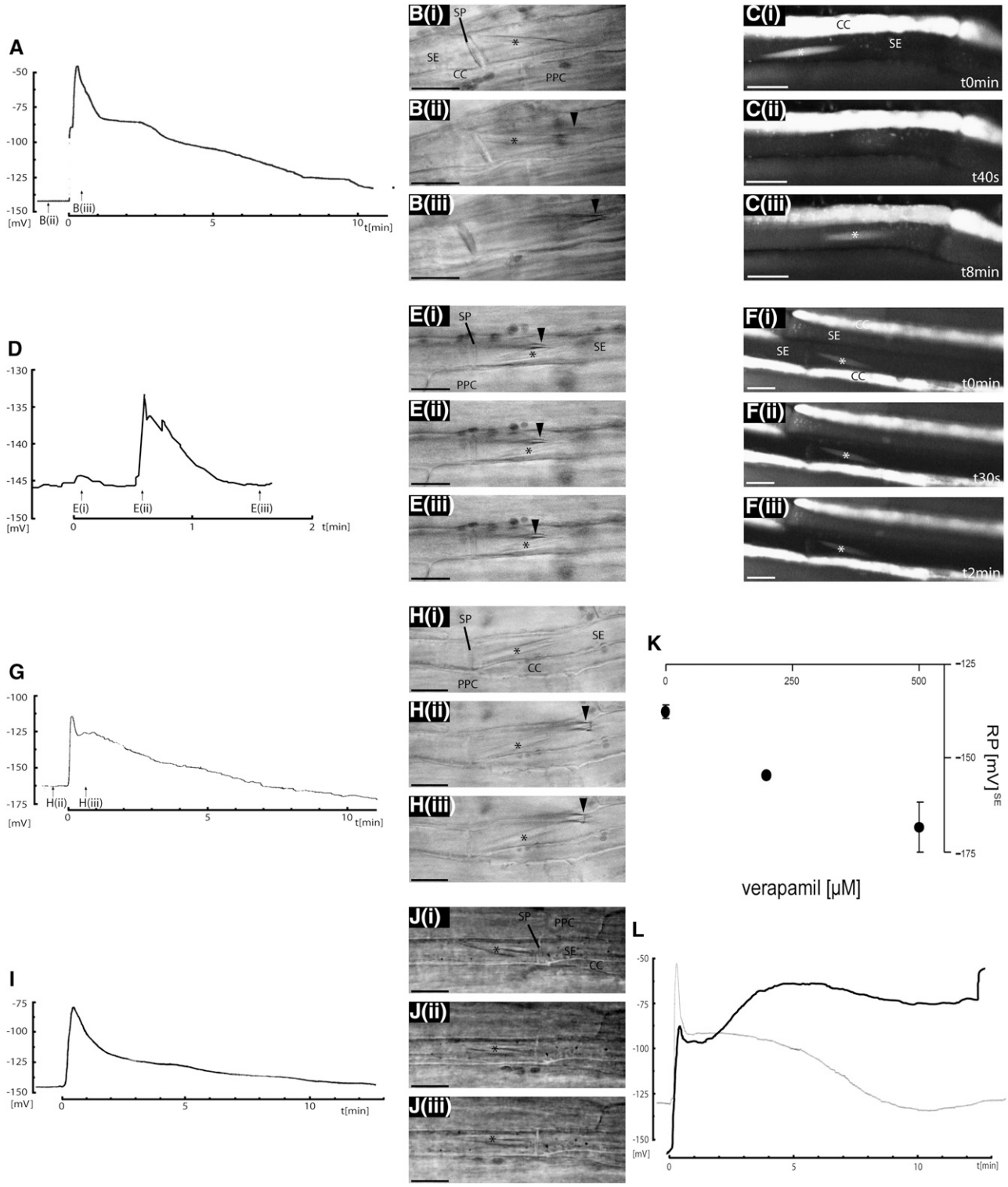

Figure 1. The Effect of Ca^{2+} Channel Blockers on EPWs and Forisome Reactions in Phloem Tissue.

Membrane potentials in SEs were recorded using microelectrodes (**[A]**, **[D]**, and **[G]**) simultaneously with microscopy observation of forisome reactions during the passage of an EPW in response to a remote burning stimulus (**[A]** to **[C]**), remote depolarization induced by 100 mM KCl (**[D]** to **[F]**), and burning in the presence of 2 mM La^{3+} (**[G]** and **[H]**). Selected bright-field images (**[B]**, **[E]**, and **[H]**) are shown at the time points indicated by arrows. In case of burning in the presence of 250 μM nifedipine, recording of EPW **(I)** and microscopy observation of the forisome **(J)** were performed in a separate

OGB-1 or Fluo-3 into intact phloem tissue, as judged by diffuse fluorescence in the densely cytoplasmic CCs, a good marker for cytosolic distribution. Labeling of the SEs showed fluorescence around the periphery of the cell in the unstirred mictoplasmic layer along the SE-PM and at the sieve plate, which is protected from the phloem stream by the overlying SER. The tissue remained viable, as judged from the continuation of rapid cytoplasmic streaming of plastids. Nevertheless, there were some differences in probe distribution. Tissue loaded with AM esters showed additional fluorescence accumulation over time in other cytoplasmic compartments, probably through continued uptake and internal cleavage of the AM ester groups, leading to punctuate staining, and some labeling of vacuoles in cells other than the SEs. By contrast, tissue loaded at low pH showed good intracellular fluorescence distribution in CCs but required more extensive washing to remove the free acid form of the dyes from the cell walls. The removal of apoplastic dye was determined by the absence of fluorescence from the lumen of cut cells adjacent to the phloem tissue. Nevertheless, it is possible that some free dye remained bound to the cell wall.

While it would be desirable to use ratiometric Ca^{2+} indicators for such measurements, it was not possible to load phloem tissue with Fura-2 or Fura-Red either as AM esters, at low pH, or following microinjection. Without the benefit of ratiometric Ca^{2+} measurements, it was important to have tight control over changes in the amount of dye, its subcellular location, the optical path length, and the amount of photobleaching, which may all result in changes in fluorescence intensity independently of any changes in cytosolic-free Ca^{2+} (Fricker et al., 1999; Camacho et al., 2000). We therefore developed a set of imaging protocols designed to minimize the effects of tissue movement and photobleaching on single wavelength measurements.

Tissue movements are an inevitable consequence of pressure waves arising from burning. To ensure that the fluorescence signals were consistently drawn from the same part of the cell, images were initially collected as three-dimensional (*x,y,z*) stacks of optical sections at 20- to 40-s time intervals to give four-dimensional (4-D) (*x,y,z,t*) image series. Specific image planes were then manually selected, typically to include the forisome in the corresponding transmission images (Figures 2A to 2E), averaged in *z* with the two adjacent optical sections and then automatically aligned over time by cross-correlation to yield a completely registered (*x,y,t*) time series (Figure 2A'). The decay in the total fluorescence intensity prior to addition of a stimulus was fit with a monoexponential curve to determine the intrinsic bleaching rate for each time series (Figure 2G) and used to correct the intensity values to compensate for photobleaching. In general, bleaching rates varied from 0.05 to 0.2% s^{-1} for OGB-1 depending on the pixel dwell time, number of optical sections per stack, and sampling frequency. Bleaching rates for Fluo-3 were significantly greater than for OGB-1, so most experiments were conducted with OGB-1. Finally, images (Figures 2B' to 2E') and measurements from specific regions of interest (ROIs; Figure 2F) were expressed as the fold change (see Methods) from the fluorescence intensity immediately prior to the stimulus (Figure 2H). In some experiments, high levels of external Ca^{2+} were added at the end of the experiment to drive the intracellular indicator to its maximum fluorescence value (e.g., Figures 2F and 2H). This indicated a maximum fold change in vivo of ~2.6-fold above resting levels for OGB-1 (Figure 2H). This is consistent with the theoretical expectations from the in vitro spectra with a resting cytosolic Ca^{2+} of ~100 nM.

While it was not possible to achieve a full Ca^{2+} calibration in intact tissues, to confirm that internal OGB-1 was fully Ca^{2+} responsive with similar sensitivity to in vitro titration conditions, the Ca^{2+} sensitivity for OGB-1 was measured in sieve element protoplasts (SEPs), as these were easier to manipulate using ionophores compared with SEs and CCs in intact tissue (Figures 2I to 2K). SEPs were isolated from *V. faba* transport phloem (Hafke et al., 2007) and loaded with OGB-1AM. Ca^{2+}-dependent fluorescence was recorded in number of SEPs using low-intensity laser scans to minimize photobleaching of OGB-1AM as described before for Fluo-3 (Plank and Sussman, 2003). For calibration, SEPs loaded with OGB-1AM taken from the same protoplast batch used for measurement were permeabilized by the Ca^{2+} ionophore ionomycin to allow intracellular/extracellular Ca^{2+} equilibration. Protoplasts were calibrated using standards with defined free Ca^{2+} concentrations according to a protocol designed for one-wavelength Ca^{2+} indicators (Plank and Sussman, 2003).

The fluorescence intensity from optical sections of SEPs loaded with OGB-1AM increased when equilibrated with different external Ca^{2+} concentrations using 4 μM ionomycin to permeabilize the PM to Ca^{2+} (Figures 2I to 2K). Forisome staining or intensive fluorescence near the PM from adherent compartments were excluded from the calibration procedure. The averaged pixel intensity values, corrected for background, exhibited an ~10-fold change in intensity when Ca^{2+} was clamped over the range 0.01 to 1 μM (Figure 2O, $n = 7$). This compares well with the theoretical maximum of ~14-fold change expected between zero and saturating Ca^{2+}. Using this calibration, the resting Ca^{2+} concentration in SEPs was estimated as 35 ± 15 nM (Figures 2P and 2Q, $n = 7$). It is noteworthy that the forisomes did not disperse during the calibration at the highest Ca^{2+} concentration (1 μM) used (Figures 2L to 2N). As an independent approach to confirm that resting Ca^{2+} was indeed low and comparable to resting levels in other cell types, we also measured free Ca^{2+} using Ca^{2+}-selective electrodes in picoliter droplets of pure phloem sap

Figure 1. (continued).

approach. For better visualization of forisome dynamics in response to distant burning **(C)** and KCl stimulus **(F)**, forisomes were also labeled with CMEDA/CMFDA. The arrowhead (**[B]**, **[E]**, and **[H]**) indicates the tip of the microelectrode for membrane voltage recording. Asterisks mark the condensed forisomes. CC, companion cells; PPC, phloem parenchyma cell; SP, sieve plate. Verapamil, representing a different class of animal L-type Ca^{2+} channel blocker, caused hyperpolarization of the resting potential ($RP_{SE} \pm SD$; **[K]**) and limited inhibition of the early phase of the EPW (**[L]**, black trace, 500 μM verapamil) in comparison to the absence of the inhibitor (L, gray trace). Bars = 10 μm.

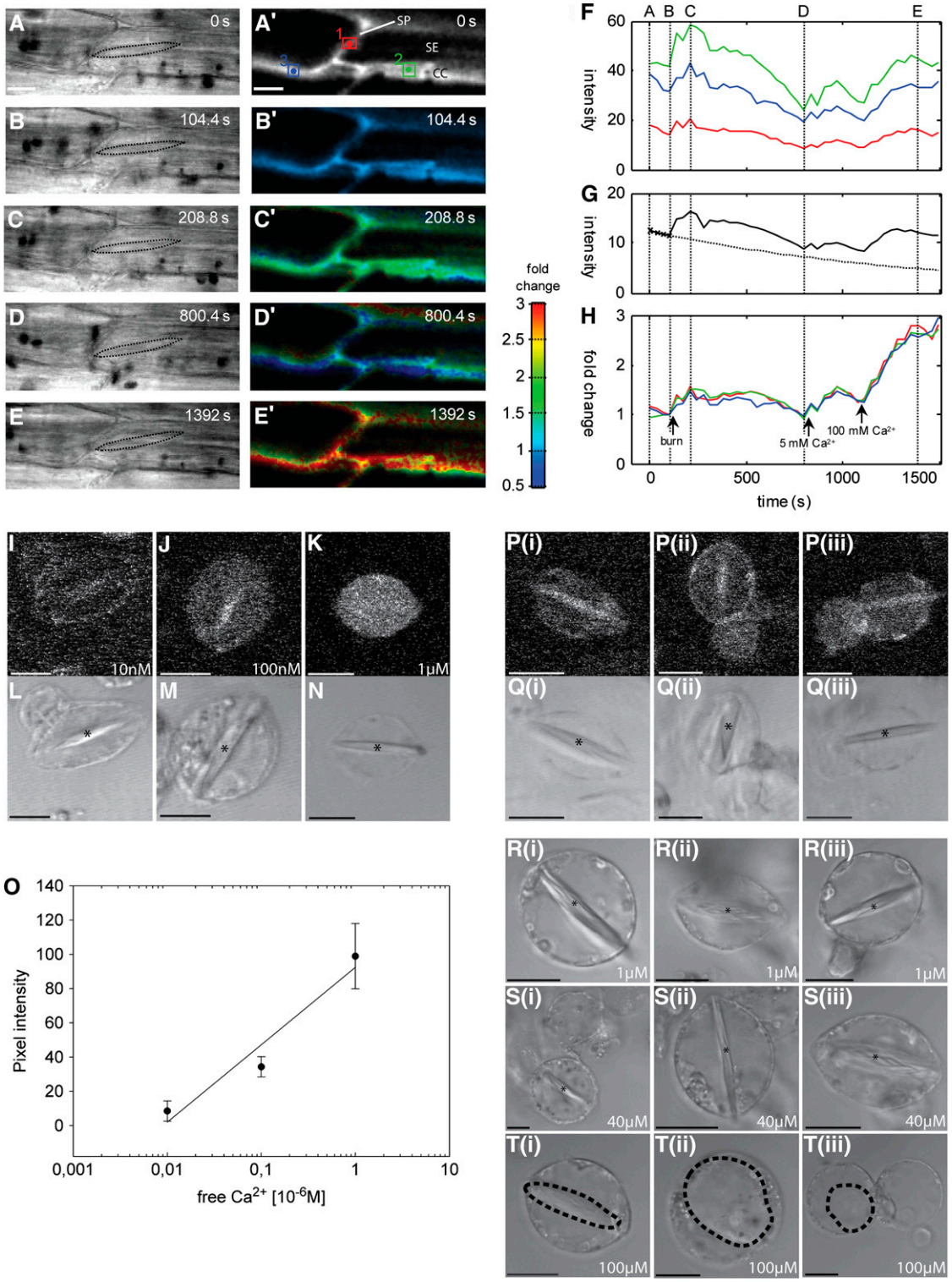

Figure 2. In Vivo Estimation of Resting Ca^{2+} Levels in Intact Phloem and SEPs Using OGB-1 and CLSM.

Transmission bright-field images with stippled contours of the forisome (**[A]** to **[E]**) and confocal optical sections of OGB-1 fluorescence (**[A']** to **[E']**) from 4-D (*x,y,z,t*) images were aligned in *x,y* and *z* to give a completely registered time series and converted to floating-point format for all subsequent operations. Following subtraction of background signals, a bleaching correction was determined from a monoexponential fit (dotted line) to the trend in the total intensity before the stimulus (solid line) **(G)**. Corrected images were normalized to a reference image, taken immediately prior to the burning

following aphid stylectomy. With this approach, free Ca^{2+} concentrations in the range of 40 to 70 nM ($n = 4$) were found for sieve tube sap.

We infer that OGB-1 provides a useful Ca^{2+} indicator with a reasonable dynamic range for phloem tissues in vivo. The calibrated measurements in SEPs and fold change observed following artificial elevation of internal Ca^{2+} are consistent with a low resting level of Ca^{2+} in these tissues. We also infer from the full dynamic range observed that the contribution of any remaining wall-bound dye was negligible. Any external dye would be saturated with Ca^{2+} at apoplastic Ca^{2+} resting levels of ~60 μM in *V. faba* (Felle et al., 2000) and would not respond further to elevated external Ca^{2+} (although fluorescence would also be quenched in the buffered medium at pH 5.7). This ought to provide a constant offset that would reduce the dynamic range of the response. However, this was not observed. The data also indicate that relatively high Ca^{2+} concentrations may be required in vivo to trigger forisome dispersion, as already observed in vitro (Knoblauch et al., 2005).

We therefore took advantage of the SEP system to facilitate manipulation of internal Ca^{2+} concentrations in the presence of ionomycin (Figures 2R to 2T) to confirm that substantial increases in Ca^{2+} were required for forisome dispersion in vivo. Up to an external Ca^{2+} concentration of 40 μM, forisomes stayed in the condensed state (Figure 2S), but forisomes did disperse when the external Ca^{2+} concentration was raised further to 100 μM (Figure 2T).

Burning Stimuli Trigger Transient Increases in Ca^{2+}

An increase in free Ca^{2+} was detected in phloem tissue after burning the leaf tip using OGB-1 and CLSM ($n = 14$). In some experiments, peak responses were observed within 60 s and were followed by an extended plateau over a period of 10 min (Figuress 2H and 3A to 3H), strongly reminiscent of the kinetics of EPWs in response to burning (Figure 1A). In other cases, the increase in Ca^{2+} was more gradual, peaking several minutes after the original stimulus was applied (Figures 3I to 3P). There was relatively little difference in the kinetics of the responses between SEs, CCs, or phloem parenchyma cells in each experiment, although the response from the SEs and CCs was marginally greater in amplitude. Across all experiments, the amplitude was quite variable, ranging from ~1.5-fold (see Figures 2C', 2H, 3C', and 3H) to >2-fold (Figures 3I' to 3M' and 3P). Assuming resting Ca^{2+} levels were in the range of 50 to 100 nM, these changes represented increases in Ca^{2+} to 200 to 500 nM.

In comparable measurements using a remote KCl application to trigger membrane depolarization, no long-term changes in Ca^{2+} were detectable in confocal time series ($n = 3$). As EPWs in response to KCl only show a rapid AP-like response, we also used rapid line scanning to achieve better temporal resolution over 4-D image collection. Following a shift from 2 to 100 mM KCl, there was a gradual rise in intensity over ~20 s followed by a return to resting levels by 40 s (see Supplemental Figure 3 and Supplemental Methods 1 online). The relative magnitude of the change was small, in the order of a 20% increase. This would equate to an increase in free Ca^{2+} of <50 nM.

Despite the transient increases in Ca^{2+} observed, particularly with the burning stimuli, no forisome dispersion was observed in any of the experiments in which tissue was loaded with OGB-1 ($n = 14$), consistent with the much higher threshold identified in the SEPs (Figure 2T). In stimuli with the lowest amplitude, the forisomes remained associated with the sieve plate and barely altered position during the Ca^{2+} response (e.g., Figures 2A to 2E). This contrasts with dispersion of 84% of forisomes in this location in unlabeled tissues ($n = 45$; see Figure 4B). In SEs with larger Ca^{2+} changes, forisomes shifted position with the onset of the Ca^{2+} transient (Figures 3A to 3E and 3I to 3M) but still did not disperse. These data suggest that the normal coupling between EPW and forisome dispersion was specifically disrupted by the presence of the cytosolic Ca^{2+} indicator. We estimate the concentration of OGB-1 in these experiments was in the range 50 to 100 μM. As OGB-1 is not known to have any other intracellular site of action, the most parsimonious explanation is that such concentrations of a mobile Ca^{2+} buffer were sufficient to breakdown local Ca^{2+} hotspots that might be needed for forisome dispersion. This explanation is consistent with the observed disruption of Ca^{2+} gradients by mobile buffers widely reported for animal systems (Neher, 1998; Demuro and Parker, 2006).

Forisome Dispersion in Response to a Heat Stimulus Correlates with the Location inside the SE

As noted above, the majority of forisomes adjacent to the sieve plate were observed to respond to a burning stimulus in

Figure 2. (continued).

stimulus to determine the fold change in intensity and visualized using a pseudo-color scale (**[B']** to **[E']**) in which hue represents the fold change and the intensity represents the signal strength. Measurements for specific ROIs (green, blue and red boxes in **[A']**, represented by the same colors in **[F]** and **[H]**) are shown for the original averaged intensity **(F)** and as the fold change after correction for photobleaching **(H)**. A short transient was observed following a remote burning stimulus (**[C']** and **[H]**), followed by a prolonged plateau that returned to resting levels over the next 8 min (**[D']** and **[H]**). Addition of increasing levels of external Ca^{2+} was used to drive the internal Ca^{2+} to saturation **(H)**. This gave a maximum fold change of ~2.6 in vivo. More precise calibration of the OGB-1 response was achieved in SEPs, following loading with OGB-1-AM, in which internal Ca^{2+} was clamped using ionomycin to calibration solutions with increasing Ca^{2+} and fluorescence imaged using CLSM (**[I]** to **[K]**). Average intensity measurements from the cytoplasm, excluding the labeled forisome, were used to construct a calibration curve (**[O]**; $n = 7$). No forisome dispersion was observed during calibration, even at 1 μM (**[L]** to **[N]**). The in vivo calibration was used to determine the resting Ca^{2+} in the absence of ionophore (three examples of each treatment are shown in **[P]**) as 35 ± 15 nM ($n = 7$). To determine the threshold internal Ca^{2+} needed to trigger forisome dispersion in SEPs, the level of Ca^{2+} was clamped at 1, 40, and 100 μM using ionomycin (three examples are shown in **[R]** to **[T]**). Forisome dispersion (dashed lines) only occurred when the Ca^{2+} concentration was >40 μM **(T)**. Asterisks mark forisomes in the condensed state. Bars = 10 μm.

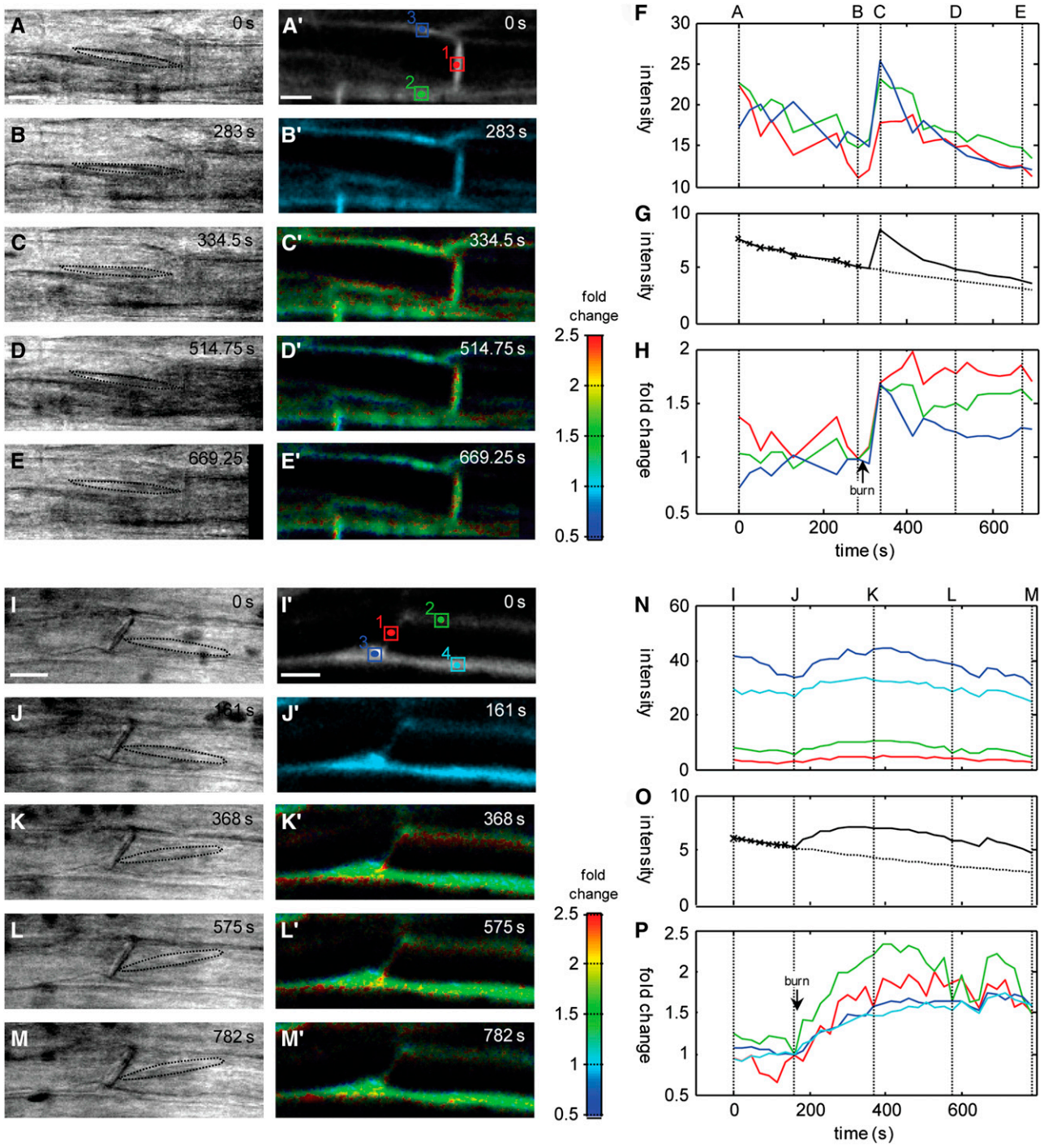

Figure 3. In Vivo Ca^{2+} Dynamics in Response to Burning Stimuli.

Different profiles of Ca^{2+} were observed in response to remote burning stimuli. In some cases (**[A]** to **[H]**; $n = 5$), there was a rapid initial response and a prolonged plateau phase. In other cases (**[I]** to **[P]**; $n = 7$), increases occurred more gradually. In some others ($n = 3$), changes were minimal. Transmission bright-field images, shown with a stippled outline around the forisome (**[A]** to **[E]**, **[I]**, and **[J]**), and confocal optical sections of OGB-1 fluorescence (**[A']** to **[E']**, **[I']**, and **[J']**) from 4-D (x,y,z,t) images were aligned in x,y and z to give a completely registered time series and converted to floating-point format for all subsequent operations. Following subtraction of background signals, a bleaching correction was determined from a monoexponential fit (dotted line) to the trend in the total intensity before the stimulus (solid line) (**[G]** and **[O]**). Corrected images were normalized to a reference image, taken immediately prior to the stimulus to determine the fold change in intensity and visualized using a pseudo-color scale (**[B']** to **[E']** and **[I']** to **[M']**), in which hue represents the fold change and the intensity represents the signal strength. Measurements for specific ROIs (boxed areas

unlabeled SEs. However, across >150 experiments, the reactivity of forisomes was variable, depending on their location in the SE, and some forisomes did not react at all. For each individual forisome that did respond, there was no correlation between the lag time following the stimulus until dispersion occurred and the subsequent time until recondensation (Figure 4A).

The propensity to disperse appeared to be related to the location of the forisome inside the SE. Forisomes were divided in four categories (Figure 4B): (1) forisomes near the sieve plate, with one end against the sieve plate and the other associated with the SE-PM; (2) forisomes with one end near the sieve plate; (3) forisomes distant from the sieve plate but with one end in the vicinity of the SE-PM; and (4) forisomes in the middle of the SE with no apparent association with the SE-PM. Eighty-four percent of the forisomes of category 1 ($n = 45$) and 70% of forisomes of category 2 ($n = 44$) dispersed in response to a distant heat stimulus (Figure 4B). By contrast, <50% of the forisomes of categories 3 ($n = 40$) and 4 ($n = 41$) reacted to burning.

Taken together with the proposal that highly localized Ca^{2+} hotspots might be required for forisome dispersion, this response profile might point to clustered Ca^{2+} stores or Ca^{2+} release channels leading to varying probabilities for forisome dispersion depending on forisome location. At the light microscopy level, attachment sites were sometimes observed between forisomes and the PM, effectively tethering the forisome in place (Figure 4C). Labeling with the ER dye, ER-Tracker Green, suggested that there was plentiful SER associated with these attachment sites (Figure 4D). At higher resolution, TEM images also highlighted close association between the forisome and clusters of stacked SER, particularly near the sieve plates (Figures 4E to 4G).

Cellular and Subcellular Localization of Ca^{2+} Channels in SEs

As a working hypothesis, we proposed that the configuration of the SER and apparent need for highly localized Ca^{2+} elevation to trigger forisome dispersion might be functionally linked if these SER stores were also endowed with a high density of Ca^{2+} channels. There are relatively few well-characterized tools available to quantify Ca^{2+} channel distributions in vivo, particularly given that it is extremely difficult to make electrophysiological measurements in phloem tissues. Nevertheless, there is evidence that the fluorescently tagged dihydropyridine, BODIPY-DHP, inhibits Ca^{2+} channels in plants through binding to voltage-sensitive Ca^{2+} channels (cf. White, 2000) and can be used to visualize Ca^{2+} channel distributions (Vallée et al., 1997). Given that nifedipine was observed to reduce EPWs (Figure 1A), we therefore tried to map DHP-sensitive channels in intact phloem tissue using fl-DHP.

Increasing concentrations of fl-DHP gave increased labeling within the SEs, particularly at the sieve plates (Figure 4H). Moreover, preincubation of intact phloem tissue in 500 μM of unlabeled nifedipine strongly reduced the fluorescence of fl-DHP, suggesting that nifedipine and the fl-DHP compete for the same binding site and does not simply reflect partitioning into a lipid environment. This has been taken to indicate that DHP is specifically binding to Ca^{2+} channels in other systems (Vallée et al., 1997). Nevertheless, nifedipine also inhibits outward K^+ channels in patch-clamp studies at higher micromolar concentrations (e.g., Terry et al., 1992; Thomine et al., 1994). Thus, to determine the specificity of binding, intact phloem tissue was titrated with increasing concentrations of fl-DHP ($n = 8$). A binding curve was obtained by plotting the fluorescence intensity of fl-DHP recorded by CLSM at each fl-DHP concentration (Figure 4I). The titration curve reveals fl-DHP binding to a high affinity system with a K_d of 600 nM. This is 10- to 100-fold lower than the K_d (5 to 90 μM) reported for nonspecific binding to K^+ channels (Terry et al., 1992; Thomine et al., 1994). There was also a suggestion of a second, even higher affinity binding system with a K_d of 40 nM. Thus, to localize putative Ca^{2+} channels in intact phloem, we used a concentration of 40 nM to reduce potential artifacts from nonspecific binding.

CLSM revealed patches of fl-DHP fluorescence at the highest density near the sieve plates (Figure 4J, insets, magnification of the sieve plate region) and along the PM of SEs. There was insufficient spatial resolution to unequivocally attribute labeling to the PM or internal membranes. Nevertheless, the irregular shape of the fl-DHP patches projecting into the luminal side of the SE suggested that fl-DHP labeling included internal membranes, such as the ER. Equally, the apparent high density of labeling at the sieve plates could include PM localization and localization to the ER within the numerous pore plasmodesma units. We therefore used colocalization with PM and ER-specific fluorophores to characterize further the predicted channel distribution.

The PM was labeled with the potential-sensitive dye RH-414 to give an independent marker for the cell boundaries (Figure 4K). The merged image clearly shows that fl-DHP labeling channels occur inside the SE lumen, most likely associated with the SER (Sjolund and Shih, 1983), as well as the SE-PM. RH-414 is known to stain solely the PM and would be expected to be distributed evenly in the PM. This provides a convenient reference to quantify the relative distribution of fl-DHP signal in or near the PM. Thus, the Ca^{2+} channel density was approximated by division of the fluorescence intensities of fl-DHP and RH-414

Figure 3. (continued).

in **[A']** and **[I']**, represented by the same colors in **[F]**, **[H]**, **[N]**, and **[P]**, respectively) are shown for the original averaged intensity (**[F]** and **[N]**) and as the fold change after correction for photobleaching (**[H]** and **[P]**). In the first experiment, a pronounced transient was observed within 20 s of a remote burning stimulus (**[C']** and **[H]**). Measurements including the sieve plate or associated CC showed a sustained increase, while signal from an overlying phloem parenchyma cell (PPC) decayed more quickly (**[F]** and **[H]**). The other class of responses observed included a more gradual rise to an extended plateau (**[I]** to **[P]**). In this case, responses including the SE and CC and PPC showed similar kinetics, but the amplitude was marginally greater from the SE/CCs **(P)**. The maximum fold change observed in the experiments shown here was ~2- to 2.5-fold, which corresponds to an increase in Ca^{2+} up to ~500 nM.

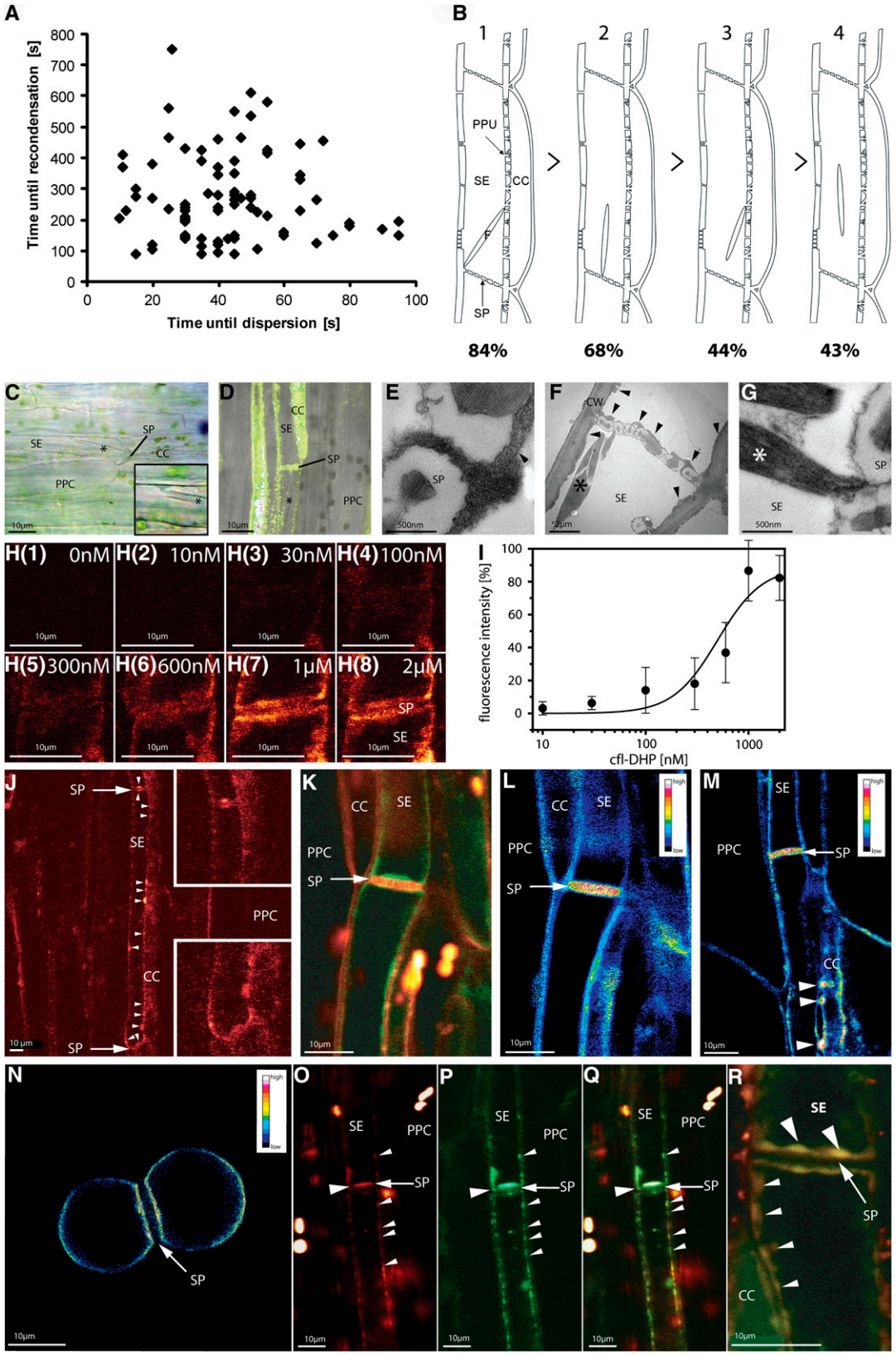

Figure 4. Relationship between Forisome Position and Responsiveness to Stimuli and Localization of Ca^{2+} Channels in SEs of *V. faba* Main Veins.

(Schild et al., 1995). The ratio fl-DHP/RH-414 image is presented in pseudocolor for intact phloem tissue (Figures 4L and 4M) as well as for an isolated twin SEP (Figure 4N; cf. Hafke et al., 2007). In all cases, a high ratio was specifically associated with the sieve plate and the pit fields connecting the SEs with the CCs, suggesting the absolute numbers of DHP-sensitive channels are higher in these regions.

Using a similar approach, we colocalized fl-DHP fluorescence with ER membrane labeled with ER-Tracker Red (Figures 4O to 4Q). Figure 4O (red channel) shows fl-DHP staining and Figure 4P (green channel) ER-Tracker Red staining of intact phloem tissue. The merged image (Figure 4Q) shows a high degree of overlap in the two signals, suggesting that DHP-sensitive Ca^{2+} channels and SER are colocalized in clusters at the sieve plate region and along the SE, mostly at the junction with the CCs (Figure 4R).

DISCUSSION

Changes in Cytosolic-Free Ca^{2+} Accompany EPWs in SEs and CCs

We showed that the free Ca^{2+} concentrations in SEs and CCs are $\leq$100 nM using two independent techniques. These values are significantly lower than previous estimates in the micromolar range (Brauer et al., 1998) but match well with cytoplasmic free Ca^{2+} concentrations of 10 to 200 nM reported for other plant systems (Plieth et al., 1999; Trewavas, 1999; Mithöfer and Mazars, 2002; Logan and Knight, 2003).

Such low resting Ca^{2+} levels are a prerequisite for Ca^{2+} to act in conventional signaling cascades, and we have demonstrated that Ca^{2+} increases occur in the SE/CC complex and adjacent cells following burning stimuli, with similar profiles and kinetics to EPWs measured in parallel experiments. The average Ca^{2+} increases in the SE/CC complex observed during burning responses reached only a few hundred nanomolar (200 to 500 nM), similar in magnitude to Ca^{2+} changes in response to hypo- and hyperosmotic treatments in *Arabidopsis thaliana* (Plieth, 2001) and duration to heat responses in tobacco (*Nicotiana tabacum*; summarized in Malho et al., 1998).

By contrast, only a brief AP, small transient change in Ca^{2+}_{cyt} (< 50 nM) and no forisome dispersion was detected in SE/CC after PM depolarization by remote application of KCl. Taken together (Figures 2H and 3P; see Supplemental Figure 3 online), these data provide the evidence that the stimulus strength is reflected in the form of specific spatio-temporal Ca^{2+}_{cyt} elevations (for review, see Ng and McAinsh, 2003; McAinsh and Pittman, 2009).

Ca^{2+} Channels Act as Relay Stations between Remote Stimuli and Occlusion Response

The inhibitory effect of a range of Ca^{2+} channel blockers, particularly membrane-impermeant La^{3+} (Figure 1G), on the amplitude

Figure 4. (continued).

(A) Time correlation between forisome dispersion in response to distant burning of the leaf tip of intact *V. faba* plants and forisome recondensation. The time points on the *x* axis indicate the lag before forisome dispersion after the remote burning stimulus. Those on the *y* axis represent the recondensation time after burning stimulus was applied.

(B) The relationship between forisome reactivity and forisome position inside SEs as identified by microscopy. Different positions are coded by numbers: (1) forisome with one end attached to the sieve plate (SP) region and the other end to the SE-PM), (2) forisome with one end attached to the SE-PM in the SP region, (3) forisome with one end attached to the SE-PM at the CC side, and (4) forisome positioned remote from the SP with no apparent attachment to the SE-PM. The percentage of forisomes dispersing in response to distant burning is given for each category.

(C) Attachment of forisomes in intact phloem tissue in the *V. faba* main vein visualized using light microscopy. The forisome (asterisk) has one forked end attached to SER and the other to the SP. The inset shows a higher magnification of the attachment of forisome forks to the SER.

(D) Overlay of phloem tissue stained with ER-Tracker green (green) and the transmission picture of SEs as recorded by CLSM. The forisome (asterisk) is attached to the SP.

(E) to **(G)** High-magnification electron micrograph ($\times$8600) of well-preserved *V. faba* SEs. Deposits of stacked ER cisternae (**[E]** and **[F]**; arrowheads) occur near the SP and are attached to the PM. The large forisome (F; asterisk) in the SE is in the condensed state. The sieve pores possess callose collars due to the section plane. CW, cell wall.

(H) Binding of the fluorescent Ca^{2+} channel inhibitor DM-BODIPY-DHP (fl-DHP) to the SP region of intact *V. faba* tissue. Representative titration (one out of eight) with various concentrations (0 to 2 μM) of fl-DHP as indicated in the micrographs.

(I) Titration curve. Plot of the measured fl-DHP fluorescence intensity (averaged pixel density) recorded from the SP region (see **[H]**) versus different fl-DHP concentrations (n = 8). Pixel density values were corrected for background. The titration curve was fitted by a Hill equation revealing a high-affinity fl-DHP binding system with K_d values of 600 nM.

(J) CLSM micrograph of *V. faba* phloem tissue, stained with the fluorescent Ca^{2+} channel inhibitor (red color) DM-BODIPY-DHP (fl-DHP). Insets show a higher magnification of both SP regions.

(K) Subcellular distribution of Ca^{2+} channels in double-stained SEs (RH-414, red; BODIPY-DHP, green) observed by CLSM. Ca^{2+} channels are localized in clusters bearing similarity to SER distribution.

(L) to **(N)** Ratio images of intact phloem tissue (**[L]** and **[M]**) and isolated SE protoplasts **(N)** are presented as pseudo-colors, obtained by division of the measured fluorescence intensities of BODIPY-DHP by RH-414. **(L)** represents the ratio image of **(K)**. Highest Ca^{2+} channel frequency was observed at SPs and at pore plasmodesma units (**[M]**; arrowheads).

(O) to **(R)** Localization of BODIPY-DHP (red, Ca^{2+} channels) **(O)** and ER-Tracker Red (green, ER) **(P)**. An overlay results in a yellowish color **(Q)**. Colocalization of fl-DHP and SER in an independent micrograph in the SP area **(R)**. Large arrowheads mark the colocalization of ER and Ca^{2+} channels at the SP and small arrowheads the colocalization of ER and Ca^{2+} channels near the PM. The direction of translocation is from top to bottom in all pictures. PPC, phloem parenchyma cell.

of EPWs recorded from *V. faba* SE/CC complex was consistent with a requirement for external Ca^{2+} influx during both the early transient AP-like phase of the phloem EPW and the prolonged VP-like depolarization phase. Besides La^{3+} (Figure 1H), Gd^{3+} (see Supplemental Figure 1 online) acts as a potent inhibitor for Ca^{2+}-dependent forisome dispersion in intact *V. faba* tissue, as previously shown for isolated SEPs (Hafke et al., 2007).

While the propagation of APs involves recruitment of PM voltage-dependent Ca^{2+} channels (cf. White, 2000; Demidchik and Maathuis, 2007), osmo-sensitive PM Ca^{2+}-conducting channels (Knoblauch et al., 2001; Hafke et al., 2007; Zhang et al., 2007) may also operate during VP in response to the hydraulic pressure wave (Stahlberg and Cosgrove, 1997). Despite the importance of PM Ca^{2+} channels in AP-like responses, there is also good evidence that propagation of APs in other systems is strongly dependent on additional release from internal stores (Plieth et al., 1999). As SEs lack vacuoles, the SER is the most obvious candidate to act as a major internal Ca^{2+} store in SEs (Sjolund and Shih, 1983; Arsanto, 1986). We showed that EPWs were inhibited by the membrane-permeant Ca^{2+} channel blocker nifedipine and that a fluorescent derivative of nifedipine (fl-DHP), known to bind to voltage-sensitive Ca^{2+} channels in animals (e.g., Knaus et al., 1992), specifically labeled ER membranes when applied at extremely low concentrations.

In vivo binding of fl-DHP was abolished by excess unlabeled nifedipine and showed high affinity binding (K_d 600 nM; Figure 4I). The K_d is significantly lower than binding of nifedipine to outward K^+ channels that are present on the PM of SE (Hafke et al., 2007), which show K_d values in the range 5 to 90 μM (Terry et al., 1992; Thomine et al., 1994). We infer that binding of fl-DHP is specific to Ca^{2+} channels in *Vicia* SE/CCs, as suggested for other plant tissues (Vallée et al., 1997; Volk and Franceschi, 2000). Maps of fl-DHP binding showed substantial concentration of putative Ca^{2+} channels at pore plasmodesma units and SE-CC junctions (Figures 4L and 4M) and colocalized with fluorescent ER markers. This latter observation is consistent with reports of fl-DHP binding to voltage-gated ER Ca^{2+} channels in crystal idioblasts of *Pistia stratiotes* (Volk et al., 2004).

DHP-sensitive Ca^{2+} channels reside on both the PM and SER in the SE-CC complex. Although the functional significance of the DHP-sensitive channels in the overall response is not yet clear, the similarity between Ca^{2+} kinetics and the long-lasting plateau phase of the EPW (Figures 1A and 1L) suggests a temporal correlation between Ca^{2+} and prolonged depolarization. While cell-impermeant La^{3+} appeared to preferentially inhibit the initial AP-like phase and had relatively little effect on the plateau, nifedipine gave a pronounced reduction in plateau phase of the EPW. We infer that nifedipine may enter the cell and bind to SER Ca^{2+} channels, as suggested from fl-DHP binding studies (Figure 4). This may result in suppression of Ca^{2+} release from SER and a reduction in internal signal.

Forisomes Must Be Tethered in the Vicinity of High Ca^{2+} Channel Concentration for Full Responses

In the absence of a cytosolic Ca^{2+} indicator, the majority (84%) of forisomes near the sieve plate dispersed in response to a burning stimulus (Figure 4B). Conversely, in the presence of OGB-1, no forisome dispersion was ever observed, and the most marked response was limited to rapid lateral movement or translocation of the forisome. Inhibition of dispersion was specifically associated with Ca^{2+} dyes, rather than arising as a general consequence from laser illumination during confocal imaging or dye toxicity (e.g., Camacho et al., 2000), as forisome dispersion occurred normally in a wide range of other imaging and labeling regimes.

One plausible explanation for both the low Ca^{2+} elevations observed and the inhibition of forisome response is that OGB-1 acts as a mobile Ca^{2+} buffer and collapses any locally high Ca^{2+} gradients that are needed to trigger forisome dispersion. Consistent with this view, we confirm here that high (> 50 μM) Ca^{2+} concentrations (Figures 2R to 2T) are needed for forisome dispersion in vivo as observed in vitro (Knoblauch et al., 2005).

Dispersion of local Ca^{2+} hot spots is well established in animal systems (Bolsover and Silver, 1991; Neher, 1998; Demuro and Parker, 2006) and can be observed with dye concentrations as low as 10 μM. There is less data specifically for plants, but loading with BAPTA buffers at comparable concentrations to OGB-1 used here is known to dissipate standing Ca^{2+} gradients in pollen tubes (Miller et al., 1992; Pierson et al., 1994) and *Fucus* rhizoids (Speksnijder et al., 1989; Taylor et al., 1996).

Current models of Ca^{2+} channel behavior suggest that very high (100 μM) localized Ca^{2+} increases can occur in the vicinity of the Ca^{2+} channel pore (Trewavas, 1999). If no other signals than Ca^{2+} alone are needed for full response, this concentration might normally be sufficient to trigger forisome dispersion. However, as OGB-1 is mobile and has high affinity and fast binding kinetics, it might act to dissipate these local gradients. Diffusion and dissociation of the dye Ca^{2+} complex would be measured as a lower and more gradual increase in Ca^{2+} throughout the cytoplasm.

A corollary of this proposal is that the forisomes might be expected to reside in close physical proximity to Ca^{2+} channel pores to experience a sufficiently high Ca^{2+} concentration. Several observations suggest the precise location of the forisome on both a macro and micro scale was critical to its responsiveness. The chance of dispersion in response to burning depended on the forisome position within the SEs (Figure 4B) and increased with proximity to the sieve plate where the highest frequencies of Ca^{2+} channels were observed (Figures 4J to 4R). Furthermore, the more intimately forisomes were associated with SER and/or the PM, the greater the probability of dispersion. The forisome ends, which are frequently forked, were sometimes observed at the TEM level to be tethered to the PM or to the SER stacks or often inserted into the ER interstices (Figures 4C to 4G). This configuration provides narrow spaces between SER stacks (Sjolund and Shih, 1983; Ehlers et al., 2000) that form an unstirred layer, in which Ca^{2+} levels may increase rapidly to high levels. The close physical proximity between PM and SER in these regions may also contribute to coupling between the initial PM depolarization and Ca^{2+} release from the ER via some form of mechanical or electrical coupling (Hepler et al., 1990). In SEs, SE-PM and SER are linked by protein anchors of unknown composition with a length of ~7 nm (Ehlers et al., 2000). Thus, voltage changes in the one membrane may be transmitted to the other membrane and influence voltage-activated Ca^{2+} channels there (Klüsener et al., 1995; Klüsener and Weiler, 1999). Alternatively,

Ca^{2+} influx through the SE-PM may trigger Ca^{2+}-induced Ca^{2+} release from putative Ca^{2+}-dependent Ca^{2+} channels, analogous to the situation reported so far for PM to tonoplast coupling (Bewell et al., 1999; Sanders et al., 2002).

METHODS

Plant Material

Plants of *Vicia faba* cv Witkiem major (Nunhems Zaden) were cultivated in pots in a greenhouse at 20 to 30°C, 60 to 70% relative humidity, and with a 14/10-h light/dark regime. Supplementary lighting (model SONT Agro 400 W; Phillips) was used to give an irradiance level of 200 to 250 $\mu mol^{-2}\ s^{-1}$ at the plant apex. Plants were used 17 to 21 d after germination in the vegetative phase just before flowering.

Preparation of Intact Plants for Electrophysiology and Observation by CLSM

For in vivo observation of sieve tubes, cortical cell layers were removed to create an observation window on the phloem from the abaxial side of the main vein of a mature leaf that was still attached to the intact plant. The cortical tissue was locally removed by manual paradermal slicing with a fresh razor blade, while avoiding damage to the phloem (Knoblauch and van Bel, 1998). The distance between the observation window and the leaf tip where stimuli were applied was 3 to 4 cm. In experiments with a KCl stimulus (100 mM KCl, 1 mM $CaCl_2$, 1 mM $MgCl_2$, and 5 mM MES/NaOH, pH 5.7) two paradermal windows 3 cm apart were cut according to Knoblauch and van Bel (1998). The KCl stimulus was applied to the apical application window and observed through the more basal observation window. The cut tissue was covered with bathing medium containing 2 mol m^{-3} KCl, 1 mol m^{-3} $CaCl_2$, 1 mol m^{-3} $MgCl_2$, 50 mol m^{-3} mannitol, and 2.5 mol m^{-3} MES/NaOH buffer, pH 5.7. In the case of the KCl stimulus, the mannitol was increased to 200 mol m^{-3} to maintain the osmotic balance. The leaf was fixed to a microscope slide with two strips of double-sided adhesive tape and mounted on the stage of a CLSM. The intactness of the phloem tissue was checked microscopically using a water immersion objective (HCX APO L40x0.80 W U-V-I objective; Leica).

Electrophysiology on Intact Phloem Tissue

Electrophysiology on intact phloem tissue was described in detail previously (Hafke et al., 2005). After submersion of the exposed phloem tissue in bathing medium for 1 h, SEs were impaled with the microelectrode under continuous microscopic surveillance using a LN SM-1-micromanipulator (Luigs and Neumann). All measurements were performed at room temperature (23 to 25°C). After stabilization of the SE resting potential, a heat shock or a KCl stimulus was applied; leaf tip burning occurred at 3 to 4 cm distance from the observation window, and the KCl stimulus was applied at the application window in the two chambered system. Changes in SE membrane potential in response to the heat pulse or KCl stimulus were recorded.

Ca^{2+} channel blockers were prepared as stock solutions (50 to 100 mM in bathing medium with the exception of the stock solution of nifedipine, which was dissolved in DMSO) and diluted prior to use to the final concentration using standard bathing medium to give working concentrations of 2 mM for La^{3+} and Gd^{3+} and 100 to 500 μM for verapamil and nifedipine. Incubation times were between 2 and 3 h.

Bright-field images were taken at different times after applying the stimulus to correlate the forisome response with the passage of the EPW using a digital camera (Canon Power Shot S40) connected to a computer (Canon Digital Camera solutions disk version 8.0 software package).

Fluorescent Probes

Fluorochrome solutions were freshly prepared in bathing medium shortly before the experiments. Preparation of the solutions is described in detail in the online version of the article (see Supplemental Methods 2 online).

Confocal Microscopy of Fluorophore Distribution

Fluorochromes were imaged by CLSM using a Leica TCS 4D (Leica Microsystems) equipped with a 75-mW argon/krypton laser (Omnichrome). Tissue was observed with a water immersion objective (HCX APO L40x0.80 W U-V-I objective; Leica) in dipping mode. The exposed phloem tissue was stained with the fluorochromes for 1 to 2 h after preincubation of at least 1 h within the bathing medium.

CellTracker Yellow-Green CMEDA and CellTracker Green CMFDA (Molecular Probes), OGB-1 (Molecular Probes), DM-BODIPY dihydropyridine (fl-DHP; Molecular Probes), and ER-Tracker Green (Molecular Probes) were excited with the 488-nm line of the argon-ion laser with emission at >510 nm, while RH-414 and ER-Tracker Red were excited by the 564-nm line of the argon/krypton laser with emission at >590 nm.

Digital images were processed with Adobe Photoshop to optimize brightness, contrast, and color and to enable an overlay of the photomicrographs. For the ratio images, the fluorescence intensities of fl-DHP and RH-414 were divided using Adobe Photoshop. The obtained ratio images fl-DHP/RH-414 are presented as a 16-color scale using Image J (Image Processing and Analysis in Java; National Institute of Health).

Ca^{2+} Dynamics in Intact Phloem Tissue

Exposed phloem tissue in intact leaves was labeled by flooding the observation window with 5 μM OGB-1 in a buffer containing 2.5 to 10 mM dimethylglutaric acid at pH 4.3 for 20 to 30 min at room temperature (21°C). Tissue was washed extensively in bathing medium and then allowed to recover for 30 to 60 min until condensed forisomes were observed before a heat stimulus at 3 to 4 cm or application of 100 mM KCl 3 to 4 cm upstream from the observation window took place.

Tissue was imaged using a Zeiss LSM510 META CLSM (Carl Zeiss MicroImaging) equipped with a $\times$25 lens (Zeiss $\times$25 0.8 numerical aperture Plan-NEOFLUAR multi-immersion lens) in dipping mode. Excitation of OGB-1 was achieved with the 488-nm line of a 30 mW argon-ion laser operating with a tube current of 6.1 A and attenuated to 0.5 to 2% of full power. OGB-1 fluorescence was collected with emission at 505 to 550 nm and chloroplast autofluorescence at 690 to 711 nm. The pinhole was adjusted to give a notional optical section thickness (axial full-width at half-maximum) of 4 μm as a compromise between axial resolution and signal strength. Z-stacks of 4 to 13 optical sections were collected with a pixel dwell time of 1.6 μs and 2$\times$ line averaging and an (x,y) pixel spacing of 0.18 to 0.27 μm and sampling repeated at 20- to 40-s intervals over ~10 min. Simultaneous nonconfocal bright-field images were collected with a transmission detector.

To compensate for specimen movement in z, particularly during passage of the pressure wave following the burning stimulus, specific z-planes were extracted from each z-stack to maintain the same cellular structures in focus. In some experiments, the signal from the adjacent z-planes was averaged to reduce noise. The extracted image series was automatically aligned in (x,y) by cross-correlation with the first image in the series. Images were converted from 8 or 16 bit to floating point to avoid rounding errors during processing. All subsequent manipulations were conducted at single precision. Images were smoothed using a 5 $\times$ 5 averaging filter to reduce noise. The background signal was measured from the vacuolar regions of a phloem parenchyma cell and subtracted from each time point. The amount of photobleaching in each experiment was estimated by fitting a monoexponential decay to the total signal from each image prior to stimulus application. The inverse of this decay

function was then used to correct images throughout the time course. To determine the relative fluorescence change following a stimulus, images were ratioed against a reference image taken immediately prior to the stimulus. Ratios were calculated on a pixel-by-pixel basis and pseudo-color-coded on a rainbow hue scale, with the image intensity and saturation reflecting the fluorescence intensity.

Regions <2 SD units above background or within 10% of saturation were excluded from the ratio images and further analysis. Changes in fluorescence intensity were averaged from user-defined ROIs and used to calculate the fold change in fluorescence for specific cell types. All image processing routines were implemented in a custom MatLab (The Mathworks) available from M.D.F. on request.

Isolation of SEPs

SEPs were isolated according to Hafke et al. (2007) (see Supplemental Methods 3 online). Isolated SEPs were washed with the bathing medium (including 400 mM) and transferred into a bathing chamber before application of the fluorescent dyes and microscopy examination of fluorochrome treatments.

Ca^{2+} Concentration Measurements in Isolated SEPs

SEPs were stained with 13.25 μM of OGB-1AM for 2 h. After washing with bathing medium, SEPs were incubated in 4 μM Ca^{2+} ionophore ionomycin to permeabilize the PM for Ca^{2+} at least for 1 h. Aliquots of permeabilized SEPs were transferred into Ca^{2+} buffer solutions (CALBUF-2; WPI) containing 10 nM, 100 nM, and 1 μM free Ca^{2+} ions. Ca^{2+}-dependent fluorescence was recorded via CLSM with low-intensity laser scans to minimize photobleaching of OGB-1AM. A calibration curve was obtained by measuring the averaged pixel density from the recorded calcium images using Image J software. The resting free Ca^{2+} level in SEP lumen was determined from the calibration curve in the absence of ionomycin.

Ca^{2+} Dependence of Forisome Dispersion

SEPs were equilibrated for 30 min with Ca^{2+} buffer solutions (CALBUF-2) containing 1, 40, or 100 μM free Ca^{2+} following ionomycin treatment and imaged using light microscopy to detect forisome responses.

Stylet Droplets and Ca^{2+} Determination by Ion-Selective Electrodes

Ca^{2+}-selective microelectrodes were fabricated as described previously (Felle and Bertl, 1986; Felle, 1988, 1989). Calibration solutions in the range of 10^{-8} to 10^{-3} M free Ca^{2+} were prepared according to Tsien and Rink (1980). Calibration curves of the microelectrode yielded a linear slope of 27 to 28 mV/pCa down to pCa = 8. Measurement of Ca^{2+} from droplets of phloem sap, obtained from *V. faba* sieve tubes using microcauterized aphid stylets, was performed as described previously (Hafke et al., 2005).

Electron Microscopy

Tissue was prepared and sectioned for TEM according to Ehlers et al. (2000) (see Supplemental Methods 4 online). The region containing the phloem window (~5 mm in length) was excised immediately before embedding in Spurr's resin and polymerization for 24 h at 68°C. Ultrathin sections (90 nm) were examined at 120 kV in an EM 912 Omega electron microscope (Carl-Zeiss). Electron micrographs were scanned as gray-scale images with a Proscan slow-scan CCD camera with Esi vision 3.2 analysis (Soft Imaging Systems, Olympus).

Supplemental Data

The following materials are available in the online version of this article.

Supplemental Figure 1. The effect of the Ca^{2+} Channel Blocker Gd^{3+} on the Forisome Reaction in Phloem Tissue.

Supplemental Figure 2. The Effect of the Ca^{2+} Channel Blocker Verapamil on the Forisome Reaction in Phloem Tissue.

Supplemental Figure 3. Rapid Line Scan Measurements of Ca^{2+} Transients.

Supplemental Methods 1. Rapid Line Scan Measurements of Ca^{2+} Transients.

Supplemental Methods 2. Fluorescent Probes.

Supplemental Methods 3. Isolation of SEPs.

Supplemental Methods 4. Electron Microscopical Preparation of Phloem Tissue.

ACKNOWLEDGMENTS

We thank Rob Roelfsema, Dirk Becker (Julius-von-Sachs-Institut für Biowissenschaften, University of Würzburg, Germany), and Anne Holz (Justus-Liebig-University) for helpful discussions, Marco Reitz, Tina Henrich, and Christian Michalski (Justus-Liebig-University) for technical assistance, and Martin Hardt (Zentrale Biotechnische Betriebseinheit, Justus-Liebig-University) for introducing the electron microscopy facilities. This work was supported by grants from the Deutsche Forschungsgemeinschaft in the frame of the Schwerpunktprogramm 1108 (BE1925/8-2, 8-3, and 15-1).

Received September 8, 2008; revised June 18, 2009; accepted June 25, 2009; published July 14, 2009.

REFERENCES

Arsanto, J.P. (1986). Calcium-binding sites and phosphatase activities in sieve element reticulum and P-protein of chick-pea phloem. A cytochemical and X-ray microanalysis survey. Protoplasma **132:** 160–171.

Bewell, M.A., Maathuis, F.J.M., Allen, G.J., and Sanders, D. (1999). Calcium-induced calcium release mediated by a voltage, activated cation channel in vacuolar vesicles from red beet. FEBS Lett. **458:** 41–44.

Bischofberger, J., and Schild, D. (1995). Different spatial patterns of [Ca^{2+}] increase caused by N- and L-type Ca^{2+} channel activation in frog olfactory bulb neurons. J. Physiol. **487:** 305–317.

Bolsover, S., and Silver, R.A. (1991). Artifacts in calcium measurements: Recognition and remedies. Trends Cell Biol. **1:** 71–74.

Brauer, M., Zhong, W.-Z., Jelitto, T.J., Schobert, C., Sanders, D., and Komor, E. (1998). Free calcium ion concentration in sieve-tube sap of *Ricinus communis* L. seedlings. Planta **206:** 103–107.

Camacho, L., Parton, R., Trewavas, A.J., and Malho, R. (2000). Imaging cytosolic free-calcium distribution and oscillations in pollen tubes with confocal microscopy: A comparison of different dyes and loading methods. Protoplasma **212:** 162–173.

Colombani, A., Djerbi, S., Bessueille, L., Blomqvist, K., Ohlsson, A., Berglund, T., Teeri, T.T., and Bulone, V. (2004). *In vitro* synthesis of (1→3)-β-D-glucan (callose) and cellulose by detergent extracts of membranes from cell suspension cultures of hybrid aspen. Cellulose **11:** 313–327.

Demidchik, V., and Maathuis, F.J.M. (2007). Physiological roles of nonselective cation channels in plants: From salt stress to signalling and development. New Phytol. **175:** 387–404.

Demuro, A., and Parker, I. (2006). Imaging single-channel calcium microdomains. Cell Calcium **40:** 413–422.

Ehlers, K., Knoblauch, M., and van Bel, A.J.E. (2000). Ultrastructural features of well- preserved and injured sieve elements: Minute clamps keep the phloem transport conduits free for mass flow. Protoplasma **214:** 80–92.

Felle, H.H. (1988). Cytoplasmatic free calcium in *Ricca fluitans* L. and *Zea mays* L.: Interaction of calcium and pH? Planta **176:** 248–255.

Felle, H.H. (1989). PH as a second messenger in plants. In Second Messengers in Plant Growth and Development, W.F. Boss, and D.J. Morre, eds (New York: Alan R. Liss), pp. 145–166.

Felle, H., and Bertl, A. (1986). The fabrication of H^+-selective liquid membrane microelectrodes for use in plant cells. J. Exp. Bot. **37:** 1416–1428.

Felle, H.H., Hanstein, S., Steinmeyer, R., and Hedrich, R. (2000). Dynamics of ionic activities in the apoplast of the sub-stomatal cavity of intact *Vicia faba* leaves during stomatal closure evoked by ABA and darkness. Plant J. **24:** 297–304.

Felle, H.H., and Zimmermann, M.R. (2007). Systemic signalling in barley through action potentials. Planta **226:** 203–214.

Fricker, M.D., Plieth, C., Knight, H., Blancaflor, E., Knight, M.R., White, N.S., and Gilroy, S. (1999). Fluorescent and luminescent techniques to probe ion activities in living plant cells. In Fluorescent and Luminescent Probes, 2nd ed., W.T. Mason, ed (London, San Diego: Academic Press), pp. 569–596.

Fromm, J. (1991). Control of phloem unloading by action potentials in *Mimosa.* Physiol. Plant. **83:** 529–533.

Fromm, J., and Bauer, T. (1994). Action potentials in maize sieve tubes change phloem translocation. J. Exp. Bot. **45:** 463–469.

Fromm, J., and Lautner, S. (2007). Electrical signals and their physiological significance in plants. Plant Cell Environ. **30:** 249–257.

Fromm, J., and Spanswick, R. (1993). Characteristics of action potential in willow (*Salix viminalis* L.). J. Exp. Bot. **44:** 1119–1125.

Furch, A.C.U., Hafke, J.B., Schulz, A., and van Bel, A.J.E. (2007). Ca^{2+}-mediated remote control of reversible sieve-tube occlusion in *Vicia faba.* J. Exp. Bot. **58:** 2827–2838.

Gilroy, S., Bethke, P.C., and Jones, R.L. (1993). Calcium homeostasis in plants. J. Cell Sci. **106:** 453–462.

Grams, T.E.E., Lautner, S., Felle, H.H., Matyssek, R., and Fromm, J. (2009). Heat-induced electrical signals affect cytoplasmic and apoplasmic pH as well as photosynthesis during propagation through the maize leaf. Plant Cell Environ. **32:** 319–326.

Hafke, J.B., Furch, A.C.U., Reitz, M.U., and van Bel, A.J.E. (2007). Functional sieve element protoplasts. Plant Physiol. **145:** 703–711.

Hafke, J.B., van Amerongen, J.-K., Kelling, F., Furch, A.C.U., Gaupels, F., and van Bel, A.J.E. (2005). Thermodynamic battle for photosynthate acquisition between sieve tubes and adjoining parenchyma in transport phloem. Plant Physiol. **138:** 1527–1537.

Hepler, P.K., Palevitz, B.A., Lancelle, S.A., McCauley, M.M., and Lichtscheidl, I. (1990). Cortical endoplasmic reticulum in plants. J. Cell Sci. **96:** 355–373.

Hille, B. (1992). Ionic Channels of Excitable Membranes, 2nd ed. (Sunderland, MA: Sinauer Associates).

Hong, B., Ichida, A., Wang, Y., Gens, J.S., Pickard, B.G., and Harper, J.F. (1999). Identification of a calmodulin-regulated Ca^{2+}-ATPase in the endoplasmic reticulum. Plant Physiol. **119:** 1165–1175.

Kauss, H. (1987). Some aspects of calcium-dependent regulation in plant metabolism. Annu. Rev. Plant Physiol. **38:** 47–72.

Klüsener, B., Boheim, G., Liß, H., Engelberth, J., and Weiler, E.W. (1995). Gadolinium-sensitive, voltage-dependent calcium release channels in the endoplasmic reticulum of a higher plant mechanoreceptor organ. EMBO J. **14:** 2708–2714.

Klüsener, B., and Weiler, E.W. (1999). A calcium-selective channel from root-tip endomembranes of garden cress. Plant Physiol. **119:** 1399–1405.

Knaus, H.G., Moshammer, T., Friedrich, K., Kang, H.C., Haugland, R.P., and Glossman, H. (1992). In vivo labeling of L-type Ca^{2+} channels by fluorescent dihydropyridines: Evidence for a functional, extracellular heparin-binding site. Proc. Natl. Acad. Sci. USA **89:** 3586–3590.

Knoblauch, M., Peters, W.S., Ehlers, K., and van Bel, A.J.E. (2001). Reversible calcium-regulated stopcocks in legume sieve tubes. Plant Cell **13:** 1221–1230.

Knoblauch, M., Noll, G., Müller, T., Prüfer, D., Schneider-Hüther, I., Scharner, D., van Bel, A.J.E., and Peters, W.S. (2005). ATP-independent contractile proteins from plants. Nat. Mater. **4:** 353.

Knoblauch, M., and van Bel, A.J.E. (1998). Sieve tubes in action. Plant Cell **10:** 35–50.

Logan, D.C., and Knight, M.R. (2003). Mitochondrial and cytosolic calcium dynamics are differentially regulated in plants. Plant Physiol. **133:** 21–24.

Lunevsky, V.Z., Zherelova, O.M., Vostrikov, I.Y., and Berestovsky, G.N. (1983). Excitation of Characeae cell membranes as a result of activation of calcium and chloride channels. J. Membr. Biol. **72:** 43–58.

Malho, R., Moutinho, A., Van der Luit, A., and Trewavas, A.J. (1998). Spatial characteristics of calcium signalling: the calcium wave as a basic unit in plant cell calcium signalling. Philos. Trans. R. Soc. Lond. B Biol. Sci. **353:** 1463–1473.

Mancuso, S. (1999). Hydraulic and electrical transmission of wound-induced signals in *Vitis vinifera.* Aust. J. Plant Physiol. **26:** 55–61.

McAinsh, M.R., and Pittman, J.K. (2009). Shaping the calcium signature. New Phytol. **181:** 275–294.

Miller, D.D., Callaham, D.A., Gross, D.J., and Hepler, P.K. (1992). Free Ca^{2+} gradient in growing pollen tubes of *Lilium.* J. Cell Sci. **101:** 7–12.

Mithöfer, A., and Mazars, C. (2002). Aequorin-based measurements of intracellular Ca^{2+}-signatures in plant cells. Biol. Proced. Online **4:** 105–118.

Montero, M., Brini, M., Marsault, R., Alvarez, J., Sitia, R., Pozzan, T., and Rizzuto, R. (1995). Monitoring dynamic changes in free Ca^{2+} concentration in the ER of intact cells. EMBO J. **14:** 5467–5475.

Neher, E. (1998). Vesicle pools and Ca^{2+} microdomains: new tools for understanding their roles in neurotransmitter release. Neuron **20:** 389–399.

Ng, C.K.-Y., and McAinsh, M.R. (2003). Encoding specificity in plant calcium signalling: hot-spotting the ups and downs and waves. Ann. Bot. (Lond.) **92:** 477–485.

Pierson, E.S., Miller, D.D., Callaham, D.A., Shipley, A.M., Rivers, B.A., Cresti, M., and Hepler, P.K. (1994). Pollen tube growth is coupled to the extracellular calcium ion flux and the intracellular calcium gradient: Effect of BAPTA-type buffers and hypertonic media. Plant Cell **6:** 1815–1828.

Plank, D.M., and Sussman, M.A. (2003). Intracellular Ca^{2+} measurements in live cells by rapid line scan confocal microscopy: Simplified calibration methodology. Methods Cell Sci. **25:** 123–133.

Plieth, C. (2001). Plant calcium signaling and monitoring: Pros and cons and recent experimental approaches. Protoplasma **218:** 1–23.

Plieth, C., Hansen, U.-P., Knight, H., and Knight, M.R. (1999). Temperature sensing by plants: The primary characteristics of signal perception and calcium response. Plant J. **18:** 491–497.

Reynolds, E.S. (1963). The use of lead citrate at high pH as an electron-opaque stain in electron microscopy. J. Cell Biol. **17:** 208–212.

Rhodes, J.D., Thain, J.F., and Wilson, D.C. (1996). The pathway for systemic electrical signal conduction in the wounded tomato plant. Planta **200:** 50–57.

Samejima, M., and Sibaoka, T. (1983). Identification of the excitable cells in the petiole of *Mimosa pudica* by intracellular injection of procion yellow. Plant Cell Physiol. **24:** 33–39.

Sanders, D., Pelloux, J., Brownlee, C., and Harper, J.F. (2002). Calcium at the crossroads of signaling. Plant Cell **14:** 401–417.

Schild, D., Geiling, H., and Bischoffberger, J. (1995). Imaging of L-type Ca^{2+} channels in olfactory bulb neurones using fluorescent dihydropyridine and a styryl dye. J. Neurosci. Methods **59:** 183–190.

Sjolund, R.D., and Shih, C.Y. (1983). Freeze fracture analysis of phloem structure in plant tissue cultures. I. The sieve element reticulum. J. Ultrastruct. Res. **82:** 111–121.

Speksnijder, J.E., Miller, A.L., Weisenseel, M.H., Chen, T.-H., and Jaffe, L.F. (1989). Calcium buffer injections block fucoid egg development by facilitating calcium diffusion. Proc. Natl. Acad. Sci. USA **86:** 6607–6611.

Stahlberg, R., and Cosgrove, D.J. (1997). The propagation of slow wave potentials in pea epicotyls. Plant Physiol. **113:** 209–217.

Stahlberg, R., Stephens, N.R., Cleland, R.E., and Van Volkenburgh, E. (2006). Shade-induced action potentials in *Helianthus annuus L.* originate primarily from the epicotyl. Plant Signal. Behav. **1:** 15–22.

Stankovic, B., Witters, D.L., Zawadzki, T., and Davies, E. (1998). Action potentials and variation potentials in sunflower: An analysis of their relationships and distinguishing charateristics. Physiol. Plant. **103:** 51–58.

Taylor, A.R., Manison, N.F.H., Fernandez, C., Wood, J., and Brownlee, C. (1996). Spatial organization of calcium signalling involved in cell volume control of the *Fucus* rhizoid. Plant Cell **8:** 2015–2031.

Terry, B.R., Findlay, G.P., and Tyerman, S.D. (1992). Direct effects of Ca^{2+}-channel blockers on plasma membrane cation channels of *Amaranthus tricolor* protoplasts. J. Exp. Bot. **256:** 1457–1473.

Thomine, S., Zimmermann, S., van Duijn, B., Barbier-Bryboo, H., and Guern, J. (1994). Calcium channel antagonists induce direct inhibition of the outward rectifying potassium channel in tobacco protoplasts. FEBS Lett. **340:** 45–50.

Trewavas, A. (1999). Le calcium, c'est la vie: Calcium makes waves. Plant Physiol. **120:** 1–6.

Tsien, R.Y., and Rink, T.J. (1980). Neutral carrier ion-selective microelectrodes for measurement of intracellular free calcium. Biochim. Biophys. Acta **599:** 623–638.

Vallée, N., Briere, C., Petitprez, M., Barthou, H., Souvre, A., and Alibert, G. (1997). Studies on ion channel antagonist-binding sites in sunflower protoplasts. FEBS Lett. **411:** 115–118.

van Bel, A.J.E. (2003). The phloem, a miracle of ingenuity. Plant Cell Environ. **26:** 125–149.

Volk, G.M., and Franceschi, V.R. (2000). Localization of a calcium channel-like protein in the sieve element plasma membrane. Aust. J. Plant Physiol. **27:** 779–786.

Volk, G.M., Goss, L.J., and Franceschi, V.R. (2004). Calcium channels are involved in calcium oxalate crystal formation in specialized cells of *Pistia stratiotes* L. Ann. Bot. (Lond.) **93:** 741–753.

White, P.J. (2000). Calcium channels in higher plants. Biochim. Biophys. Acta **1465:** 171–189.

Zawadzki, T., and Trebacz, K. (1982). Action potentials in *Lupinus angustifolius* L. shoots. J. Exp. Bot. **33:** 100–110.

Zhang, W., Fan, L.-M., and Wu, W.-H. (2007). Osmo-sensitive and stretch-activated calcium-permeable channels in *Vicia faba* guard cells are regulated by actin dynamics. Plant Physiol. **143:** 1140–1151.